

GMM-S Diffusion: Gaussian Mixture Masks and Scaling for Diffusion Models

Chang Liu, Karim Habashy, Peter Yuchen Pan, Hadi Sepanj

December 20, 2023

Abstract

Denoising diffusion probabilistic models (DDPMs) have demonstrated superior image generation capabilities but suffer from slow inference and high computational costs. To address these challenges, we propose two novel modifications to enhance small-scale diffusion models. First, we leverage Gaussian mixture masks (GMMs) to convey a structural bias in transformer based denoising blocks during training, aiming to improve sample efficiency. Second, we explore the scaling of skip connections and denoising blocks in a U-ViT backbone to boost image generation quality without additional training. Our experiments on CIFAR-10 reveal insights into the impact of these modifications on Frechet Inception Distance (FID), training steps, and computational efficiency. While GMMs’ effectiveness requires further exploration, the scaling approach demonstrates promise in bridging the gap between small and large diffusion models, offering a pathway to adjust state-of-the-art image generation techniques.

1 Introduction

Recently, denoising diffusion probabilistic models (DDPMs) have become the focal center in the research landscape due to its stability during training and superior image generation capabilities on image, 3D, video data and beyond [1]. Compared to previous image generation frameworks such as variational autoencoders (VAE) [2] and generative adversarial networks (GAN) [3], diffusion models employ a novel image generation architecture involving a forward diffusion process and a reverse diffusion process. In the forward process, Gaussian noises are added to realistic sample images until the images become complete Gaussian noise. A neural network is trained in the reverse process to denoise at each step to map the Gaussian noise to the input sample.

However, diffusion models are also notorious for incredibly slow image generation at inference due to the need to traverse the denoising reverse diffusion chain, which involves going through the same network hundreds or even thousands of times [4]. Moreover, diffusion models require significant training data and computation time, making its benefits difficult for researchers and small-scaled businesses to leverage [4]. In fact, training DDPM [5] on eight V100 GPUs for the LSUN-Bedroom dataset [6] costs around four days at resolution 64×64 and over two weeks at resolution 256×256 [4].

At the moment, the most exciting and cutting-edge generative AI and diffusion model results are created or backed by large corporations with enormous computational power and data [4]. Unlike

the previous state of the art image generation techniques such as VAE and GANs, the current state of the art image generation technique DDPM is becoming exceedingly inaccessible to researchers and smaller scaled businesses. As a result, democratizing diffusion model is an increasingly pressing problem.

To reduce computational cost of diffusion models both during training and inference, we propose Gaussian mixture masks and scaled skip connections for Diffusion Models (GMM-S Diffusion), a model architecture that seek to improve image generation quality for small training datasets with limited added parameters. Specifically, our method involves two components, Gaussian mixture masks (GMM) and Scaled Skip connections, applied on a U-ViT backbone [7]. We replace the U-Net denoising block in DDPM with a vision transformer based variant that preserves U-Net’s long skip connections to achieve similar image generation quality with less training time. During training, we adopt an implicit structural bias by applying Gaussian mixture masks on the attention heads to improve image generation capabilities for the CIFAR-100 dataset with almost zero additional parameters and computational cost. We then scale the feature map and skip connections during inference to further boost image generation quality.

Although our method resulted in slightly higher FID score compared to the vanilla U-ViT architecture, images generated from our model contains richer semantic information. If time permitted, more experiments can be conducted as detailed in the Future Directions section.

Our project makes several noteworthy contributions, summarized below:

- We adapted U-Net based DDPM [8] to U-ViT architecture [7]¹ of the same size.
- With no additional training, we improve image generation at inference by weighing the feature maps in the denoising blocks and skip connections drawing on the strengths of each component for image generation.
- Apply a locality prior, specifically Gaussian mixture masks, during training to boost image generation capabilities for small datasets with only 2 additional parameters per mask kernel.

This report is structured as follows: First, the relevant background for our project is presented to develop a solid grounding in our approach. We then introduce our modifications to the denoising block’s architecture in the methods section. Following this, the Results and Analysis section shows our findings and their implications for image generative modelling. Finally, we conclude the report and outline interesting avenues for future works.

2 Background

2.1 Locality Prior in Transformer model

Convolutional Neural Networks (CNNS) were crafted with the compositionality of the visual world in mind [9]. The knowledge of hierarchical structure present in the objects that surround us allowed this class of models to capture semantic properties of the world.

¹As U-ViT outperforms the CNN based denoiser backbones while using less training data [7], this observation serves as the motivation here.

The seminal paper "Attention is All You Need" highlighted the importance of attention mechanisms in modeling long-range dependencies, a feature that has shown considerable promise in vision applications [10]. However, this does not imply that transformers can easily capture the local inductive biases inherent to Convolutional Neural Networks (CNNs). While transformers can eventually learn these biases and even surpass CNNs given sufficient data, this means that parameters and training samples are used up to capture/learn the inherent structure of the world [11].

Attempts have been made to leverage the global attention ability of the transformer with relevant inductive biases for performance and sample efficiency improvements. RetNet replaces the softmax operation in transformer with a Haddamard product of the attention matrix with a relative position-based exponential decay mask and GroupNorm operations for non-linearity [12]. This mask makes an assumption about the structural nature of text. Another approach adds a weighing parameter following the attention operation [13].

This concept has then been adapted to the vision domain by adapting the Vision Transformer (ViT) to incorporate a locality bias [11]. The Retentive Memory Network(RMT) and the Vision Retention Network (ViR) both apply exponentially decaying masks to the attention mechanism [14,15].

Inspired by the fact that the inductive bias of a mask can be useful, the authors of GMM initially opt to fully learn a mask without imposing a resulting shape (as opposed to the exponential decays above) [16]. This element-wise learnable mask indeed also improved performance of a vision transformer, however it did so at the cost of a significant increase in computation overhead and model size. They note down spatial characteristics of the learned masks:

- Locality: Masks had high local correlations at lower depths, global at deeper layers.
- Patches actively suppressed their attention scores to themselves.

With this, the authors proposed constructing a mask able to capture this structure, specifically though Gaussian mixture masks. These masks only require with 2 learnable parameters per kernel. Interestingly, this approach with only a few hundred extra parameters outperformed even the initial fully learnable mask approach (which necessitated hundred of thousands of extra parameters). These improvements were accentuated in tasks with limited data.

2.2 Denoising Diffusion Modelling

Diffusion models are a class of generative models typically used for image synthesis. These models learn a conditional transition from pure gaussian noise to esamples in the image domain. They are a competitive method compared to Generative-Adversarial Networks (GANs) and Variational Autoencoders (VAEs), as they have been shown to generate higher quality images compared to VAEs, while not suffering the same instabilities encountered when training GANs [17].

To train them, a forward process is applied where noise is added iteratively to an input sample (usually an image) x_0 using a Markov Chain until it is no longer distinguishable from pure noise $x_T \sim \mathcal{N}(0, I)$. To recover the original image, a neural network is trained to sequentially predict the noise and remove it from the image using the same network. Effectively, this process parameterizes the reverse diffusion process by learning an adequate sequence of conditional distributions that

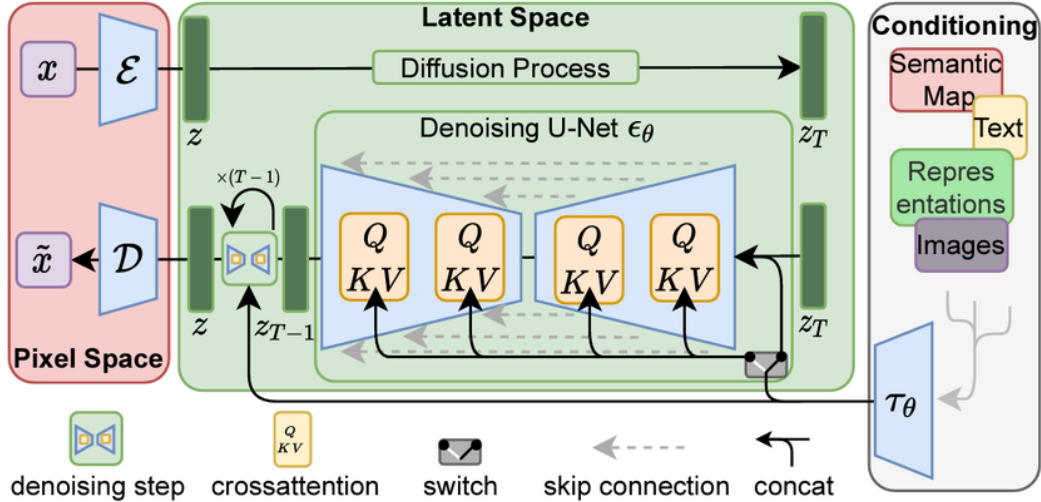


Figure 1: Training mechanism of a Latent Diffusion Model. We can see that the input and output use an AutoEncoder to go to and from a latent space, where the diffusion process is applied. Optionally, the reverse process can leverage multi-modal conditioning in this joint latent space using pre-trained frozen encoders

lead to the distribution of the original data.

Typically, the neural network architecture leveraged is the U-Net, which is a convolutional network identifiable by its encoder-decoder architecture and its skip connections. Specifically, the encoder block downsamples the image inputs, effectively capturing the high level semantics of the input. The decoder is then tasked with upsampling the representation, and returns the original dimensionality of the input. To assist with the recovery of fine grained low-level details lost in the downsampling step, long skip connections from the encoder are concatenated with the denoising decoder features. This also stabilizes training by alleviating the vanishing gradient issue.

Building on this work, Latent Diffusion Models (LDMs) [?], embed the U-Net into the latent space of a pre-trained AutoEncoder (AE). This shift to a lower-dimensional latent space means that latent diffusion models (LDMs) need significantly less computation and time to generate images. The AE allows for modelling more complex statistics of the data, further improving image quality generation. Beyond this, the latent space enables for cross-modality encoding, allowing for class and text conditioning for of the outputs. This is shown in Figure 1.

Work by Bao et al. pushes further in the direction of less reliance on the U-Net by proposing U-ViT: a transformer based denoising backbone with long skip connections between the shallow and deep layers (drawing inspiration from the original U-Net) [7]. By employing these long skip connections, low level feature information is able to propagate through the transformer layers of the denoising U-ViT, easing the pixel-level prediction objective in diffusion models.

In FreeU, the authors employ a study of the U-Net architecture and point out the significance of the information propagated through the denoising blocks and the long skip connections [18]. They note that the denoising block contributes to the generation of high level (low frequency) components

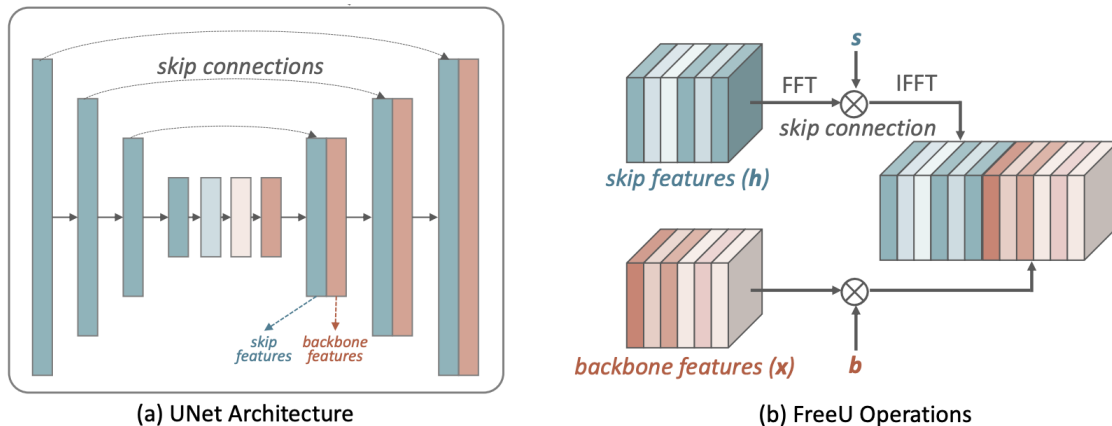


Figure 2: Depiction of the modulating factors proposed in FreeU

of the generated samples, where these generated features embody the global/smooth characteristics of an image. Conversely, the skip connections carry over the low level (high frequency) information to later layers for denoising - once the global features of the image have already been resolved. Equipped with this knowledge, the authors propose a method that, when applied during inference, can lead to improved image generation quality with no addition of *any* trainable parameters. They introduce two modulating factors for the skip connections and denoising blocks, depicted in Figure 2. The first is used to downscale the low frequency information present in skip connections, as the authors argue that low frequency present in the skip connection features may be attenuating the efficacy of the denoising blocks. Due to this removal of low frequency information from the reverse diffusion process, the second factor is employed to upscale the denoising decoder blocks.

3 Methods

In this section, we outline our approach to improving the image generation quality of a U-ViT backbone model no noticeable increase in computational requirements during training. The first step consists of adding the Gaussian mixture masking prior to the self-attention operation. In parallel to this, we apply the scaling factors used in [18] to explore to what extent the transformer denoiser with skip connections given by U-ViT operates similarly to the original U-Net. Our proposed approach can be seen in Figure 3

3.1 Gaussian mixture masks

Our method extends the GMMs to image generation within a UViT-based framework. We develop our masks in the manner outlined in Algorithm 1. The learnable parameters, α and σ , define each mask. For a given attention block, we concatenate 5 kernels (this was shown to give the best performance boost). Figure 4 illustrates the resulting mask of 5 randomly initialized kernels. In a standard transformer with 12 heads and 12 layers, this adds only a few hundred parameters to the model size - which translates to almost indistinguishable additional computation overhead.

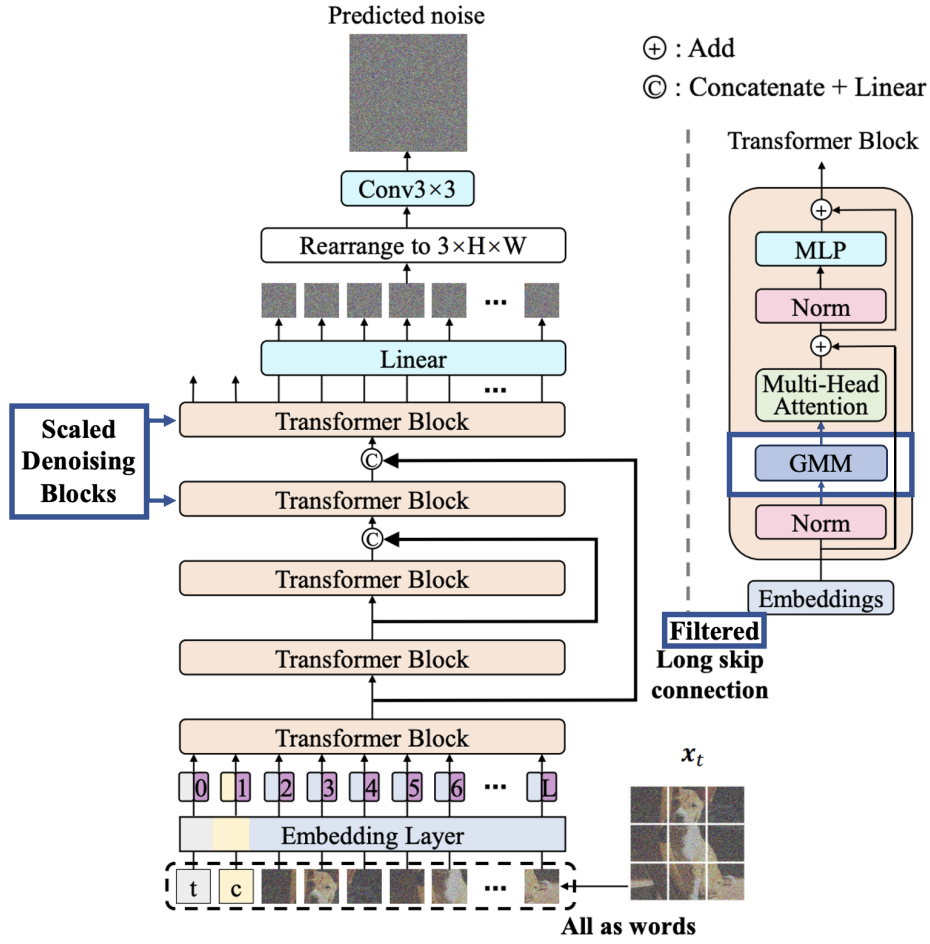


Figure 3: Our proposed architecture is based on the diffusion U-ViT, where our specific contributions can be seen in blue squares

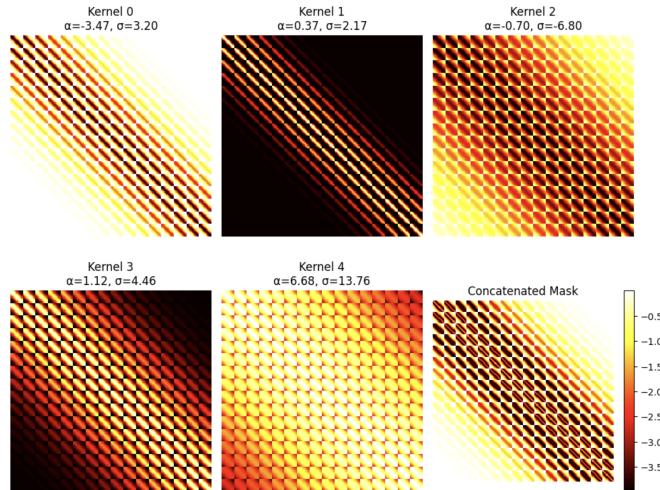


Figure 4: Example of randomly initialized Gaussian kernels. The bottom right figure shows the final GMM that would be element-wise multiplied with the patches prior to the attention operation. Intuitively, large α values will amplify information in the attention map while small/negative values will suppress it. For σ , a large value applies the weighing effects globally, while a small one operates locally.

Algorithm 1 Gaussian mixture mask

Input: Number of patches N number of Kernels K small constant ϵ **Initialization:** α_k and σ_k from normal distributions, $M_{K \times N \times N}$ **for** $i = 0$ to $N - 1$ **do** **do**

for $j = 0$ to $N - 1$ **do**

$\Delta_x = i \% N^{1/2} - j \% N^{1/2}$

$\Delta_y = i // N^{1/2} - j // N^{1/2}$

for $k = 0$ to $K - 1$ **do**

$M_{ij} += \alpha_k e^{-\frac{\Delta_x^2 + \Delta_y^2}{2\sigma_k^2 + \epsilon}}$

end for

end for

end for=0

3.2 Scaling skip connections and denoising blocks

As mentioned, we scale the denoising outer blocks and skip connection components of the denoising network. First, we apply a high pass filter to the skip connection features. To do this, we compute the Fourier Transformer of the content of the skip connection h_l to obtain the frequency information (where l is outlines the layer in question). Because the rationale for using skip connections at inference time is to supply the later layers with high frequency information, we downscale all features below some threshold value r_{thresh} by a factor s_l .

$$h'_l = \text{IFFT}(\text{FFT}(h_l) \odot \beta_l) \quad (1)$$

$$\beta_l(r) = \begin{cases} s_l, & \text{if } r < r_{thresh} \\ 1, & \text{otherwise} \end{cases} \quad (2)$$

To make up for lost information in the skip connection filtering, we amplify the scaling of the denoiser transformer blocks concatenated with the skip connections. Because we're working with a vision transformer, the features propagated through the network are not output maps from convolutional kernels, but rather fixed sized patches. Furthermore, the U-ViT model appends time and class conditioning tokens to the network as patches for simplicity. To deal with this, we omit these first 2 tokens from the scaling operation. We then determine the scaling factor α_l using a normalized average of the features of the transformer block and β_l .

$$\bar{x}_l = \frac{1}{N} \sum_{i=1}^N x_{l,i} \quad (3)$$

$$\alpha_l = (b_l - 1) \cdot \frac{\bar{x}_l - \min(\bar{x}_l)}{\max(\bar{x}_l) - \min(\bar{x}_l)} + 1 \quad (4)$$

$$x'_{l,i} = x_{l,i} \odot \alpha_l \quad (5)$$

4 Results and Analysis

In pursuit of enhancing the quality of diffusion models, we directed our research along two distinct avenues, as outlined in Section 3. The first approach involves the integration of Gaussian mixture masks with the diffusion model, aimed at augmenting image generation quality, particularly beneficial for small datasets. This enhancement is achieved with nearly zero additional parameters and minimal computational cost. Moreover, our model learns two parameters to implicitly generate Gaussian mixture masks on attention heads, further refining the generation process.

Simultaneously, the second avenue explores the efficacy of skip connections during inference. By strategically rescaling U-Net’s skip connection feature maps and backbone, we endeavored to elevate image quality without the need for additional training or fine-tuning. This technique involves adjusting two scaling factors: the first entails scaling the backbone based on averaged feature maps, while the second involves scaling long skip connections across different decoder blocks.

In the subsequent sections, we present and discuss the results stemming from our proposed methodologies, providing insights into their impact on image generation quality and computational efficiency. Through a comprehensive examination, we aim to shed light on the effectiveness of these strategies and their potential contributions to advancing the state-of-the-art in diffusion models.

4.1 GMM-Diffusion Fusion

In this section, we present the results of our experiments conducted on the CIFAR-10 dataset using the smallest U-Vit model with the modification of Gaussian mixture mask (GMM). Our objective is to compare the Frechet Inception Distance (FID) scores between the original U-Vit and the modified version with GMM. Additionally, we investigate whether the diffusion model using GMM requires fewer training steps. Furthermore, we provide insights into the computational overhead introduced by the GMM modification by calculating the Floating Point Operations per Second (FLOPs) for both models. Moreover, in the Appendix section, various figures showcase different GMMs across different layers.

While our proposed method aimed to leverage Gaussian mixture masks (GMMs) to introduce a built-in structural bias for enhanced sample efficiency, our results indicate that the performance fell short of expectations.

4.1.1 FID Scores Comparison

Table 1 summarizes the FID scores for the original U-Vit and the U-Vit with GMM. The values are computed based on the CIFAR-10 test set, higher FID scores indicate that the achieved performance did not meet initial expectations.

4.1.2 FLOPs Comparison

To evaluate the computational efficiency, we calculate the Floating Point Operations per Second (FLOPs) for both the original U-Vit and the U-Vit with GMM. Table 2 presents the FLOPs

Table 1: FID Scores Comparison

Model	Original U-Vit	U-Vit with GMM
FID Score	3.11	3.328

comparison.

Table 2: FLOPs Comparison

Model	Original U-Vit	U-Vit with GMM
FLOPs (GFLOPs)	181.34	181.34

The FID scores, training steps, and FLOPs comparisons provide valuable insights into the impact of the GMM modification on the smallest U-Vit model’s performance and computational efficiency.

4.2 Skip-Diffusion

In this section, we delve into the results derived from the approach of employing the modified weighted skip connections and denoising blocks, as described in Section 3.2. Figure 4.2 and figure 4.2 illustrate the outcomes of our experimentation (while figure 4.2 depicts the original U-ViT) in two different settings (more experiments are available in Appendix section), a qualitative discussion is brought on the impact of parameters settings on image generation through this method.

The analysis of the experimental results reveals a interplay between two key parameters, s and b within the model. Notably, when s is systematically decreased while maintaining b at a constant level, there is a degradation in the quality of image generation. This trend suggests that reducing the scaling factor s independently (i.e. significant filtering out of lower frequency information in the skip connections) has a negative impact on the overall image synthesis, potentially leading to a loss of important details or introducing undesired artifacts.

Conversely, when b is increased (more denoising per step) while s is held constant, an interesting pattern emerges. Initially, the results show an improvement in image quality, suggesting that higher values of b contribute to generating sharper and more defined images. However, beyond a certain threshold, the images become excessively sharp, potentially at the cost of losing essential details. This observation highlights the balance required when tuning the b parameter, as high values compromise the quality of the generated images.

Combining these features yields interesting results. As noted, decreasing the s parameter led to degradation of quality. Notably, however, when s is decreased with a high b parameter, it offsets the excessive sharpness in the images and restores the high quality samples.

In addition, understanding the distinct roles played by skip connections versus denoising blocks here seems to be important. Skip connections and denoising blocks constitute integral components



Figure 5: Visualizing the Impact: A showcase of image generation outcomes for each of the five classes, revealing the influence of parameters b and s on the synthesis process. Explore the variations across 25 generated samples, offering insights into the diverse outcomes achieved through the interplay of these key parameters with $b = 1.0, s = 1$

influencing the model’s ability to capture both high and low-frequency information during the denoising process. While skip connections contribute to the propagation of low-level details and facilitate the recovery of fine-grained features, denoising blocks play a crucial role in synthesizing high-level, global characteristics of the generated images. The delicate interplay between these components is essential for achieving a balance between sharpness, quality, and the preservation of details. Further exploration into the interactions and individual contributions of skip connections and denoising blocks may contain potentials to fine-tune their functionalities and enhance the performance of our model.

4.3 Conclusion and Future Work

4.3.1 Conclusion

In this work, we have presented the outcomes of our experiments conducted on the CIFAR-10 dataset, employing the smallest U-Vit model with a distinctive modification – the Gaussian mixture mask (GMM). Our primary aim was to assess and contrast the performance of the original U-Vit



Figure 6: Visualizing the Impact: A showcase of image generation outcomes for each of the five classes, revealing the influence of parameters b and s on the synthesis process. Explore the variations across 25 generated samples, offering insights into the diverse outcomes achieved through the interplay of these key parameters with $b = 1.8, s = 0.85$

against the variant incorporating GMM, with a focus on the Fréchet Inception Distance (FID) scores. Our results indicate noteworthy differences in FID scores between the two models, shedding light on the impact of the GMM modification on the model’s ability to generate realistic and high-quality images. This insight is crucial for understanding the effectiveness of GMM in enhancing the generative capabilities of U-Vit on the CIFAR-10 dataset.

Furthermore, our investigation delves into the training dynamics of the diffusion model with GMM, exploring whether this modification necessitates fewer training steps compared to its unmodified counterpart. Understanding the convergence properties and training efficiency is paramount for optimizing the training process, especially in resource-intensive tasks. Additionally, we provide valuable insights into the computational overhead introduced by the GMM modification. By calculating the Floating Point Operations per Second (FLOPs) for both the original U-Vit and the GMM-enhanced version, we quantify the computational cost associated with integrating GMM. This information is crucial for practitioners and researchers alike, as it helps in making informed decisions about the trade-off between computational complexity and model performance.



Figure 7: Visualizing the Impact: A showcase of image generation outcomes for each of the five classes, revealing the influence of parameters b and s on the synthesis process. Explore the variations across 25 generated samples, offering insights into the diverse outcomes achieved through the interplay of these key parameters with $b = 1, s = 0.85$

In conclusion, our comprehensive analysis of FID scores, training steps, and FLOPs underscores the significance of the GMM modification in the context of the U-Vit model on the CIFAR-10 dataset. These findings not only contribute to the understanding of the model’s generative capabilities but also provide practical insights for researchers seeking to leverage diffusion models with GMM in resource-constrained environments. The knowledge gained from this study is encouraging for our future work.

4.3.2 Future Directions

In light of the results achieved through this project, several suggestions for future exploration emerge.

- One direction involves extending the applicability of these scaling factors to the training phase. Specifically, during training, the skip connections currently utilize a downscaling operation on frequencies below a predefined threshold. In future investigations, an intriguing possibility lies in replacing this fixed downscaling with a dynamically learned low-pass filter,

potentially leveraging mathematical models such as Tschebyscheff [19] or Butterworth [20]. This adaptive approach could optimize the model’s ability to capture relevant frequency information, offering a trainable refinement to the denoising process. Such an exploration aligns with the objective of enhancing image generation quality without significantly increasing computational demands.

- An interesting avenue to explore would be a hybrid U-ViT/U-Net approach, where the skip connections can direct information to convolutional blocks in addition to the original skip connections. This new architecture may shed light on the differences between these models.
- One potential explanation for having a lower FID score compared to our baseline might be the fact that we applied learnable Gaussian mixture masks across each denoising timestep and block. As a result, it is possible that our network is learning solely from the noise in the earlier timesteps and the GMM never converged well. If time permitted, we would conduct experiments where we apply GMM after a few timesteps when there is less noise. It would be interesting to observe if such experiments lead to more conclusive results.
- Furthermore, a more targeted application of the masks can better leverage their benefits. For instance, we can explore avenues where we use different GMM parameters across each denoising step to account for different noise and realistic image distribution across timesteps.
- A more extensive comparison of the hidden features throughout denoising should be employed comparing the baseline, weighted skip-connections/denoising blocks, and gaussian mixture masks.
- Finally, a merging of the two methods discussed in this project would be fruitful in achieving our goal of improving diffusion models both during training as well as at inference.

References

- [1] L. Yang, Z. Zhang, Y. Song, S. Hong, R. Xu, Y. Zhao, W. Zhang, B. Cui, and M.-H. Yang, “Diffusion models: A comprehensive survey of methods and applications,” *ACM Computing Surveys*, vol. 56, no. 4, pp. 1–39, 2023.
- [2] D. P. Kingma and M. Welling, “Auto-encoding variational bayes,” *arXiv preprint arXiv:1312.6114*, 2013.
- [3] I. Goodfellow, J. Pouget-Abadie, M. Mirza, B. Xu, D. Warde-Farley, S. Ozair, A. Courville, and Y. Bengio, “Generative adversarial networks,” *Communications of the ACM*, vol. 63, no. 11, pp. 139–144, 2020.
- [4] Z. Wang, Y. Jiang, H. Zheng, P. Wang, P. He, Z. Wang, W. Chen, and M. Zhou, “Patch diffusion: Faster and more data-efficient training of diffusion models,” *arXiv preprint arXiv:2304.12526*, 2023.
- [5] J. Ho, A. Jain, and P. Abbeel, “Denoising diffusion probabilistic models,” *Advances in neural information processing systems*, vol. 33, pp. 6840–6851, 2020.

- [6] F. Yu, A. Seff, Y. Zhang, S. Song, T. Funkhouser, and J. Xiao, “Lsun: Construction of a large-scale image dataset using deep learning with humans in the loop,” *arXiv preprint arXiv:1506.03365*, 2015.
- [7] F. Bao, S. Nie, K. Xue, Y. Cao, C. Li, H. Su, and J. Zhu, “All are worth words: A vit backbone for diffusion models,” in *Proceedings of the IEEE/CVF Conference on Computer Vision and Pattern Recognition*, 2023, pp. 22 669–22 679.
- [8] R. Rombach, A. Blattmann, D. Lorenz, P. Esser, and B. Ommer, “High-resolution image synthesis with latent diffusion models,” in *Proceedings of the IEEE/CVF conference on computer vision and pattern recognition*, 2022, pp. 10 684–10 695.
- [9] Z. Yan, H. Zhang, R. Piramuthu, V. Jagadeesh, D. DeCoste, W. Di, and Y. Yu, “Hd-cnn: Hierarchical deep convolutional neural networks for large scale visual recognition,” in *Proceedings of the IEEE International Conference on Computer Vision (ICCV)*, December 2015.
- [10] A. Vaswani, N. M. Shazeer, N. Parmar, J. Uszkoreit, L. Jones, A. N. Gomez, L. Kaiser, and I. Polosukhin, “Attention is all you need,” in *Neural Information Processing Systems*, 2017. [Online]. Available: <https://api.semanticscholar.org/CorpusID:13756489>
- [11] A. Dosovitskiy, L. Beyer, A. Kolesnikov, D. Weissenborn, X. Zhai, T. Unterthiner, M. Dehghani, M. Minderer, G. Heigold, S. Gelly, J. Uszkoreit, and N. Houlsby, “An image is worth 16x16 words: Transformers for image recognition at scale,” *ArXiv*, vol. abs/2010.11929, 2020. [Online]. Available: <https://api.semanticscholar.org/CorpusID:225039882>
- [12] Y. Sun, L. Dong, S. Huang, S. Ma, Y. Xia, J. Xue, J. Wang, and F. Wei, “Retentive network: A successor to transformer for large language models,” *ArXiv*, vol. abs/2307.08621, 2023. [Online]. Available: <https://api.semanticscholar.org/CorpusID:259937453>
- [13] S. H. Lee, S. Lee, and B. C. Song, “Vision transformer for small-size datasets,” *ArXiv*, vol. abs/2112.13492, 2021. [Online]. Available: <https://api.semanticscholar.org/CorpusID:245501976>
- [14] A. Hatamizadeh, M. Ranzinger, and J. Kautz, “Vir: Vision retention networks,” *ArXiv*, vol. abs/2310.19731, 2023. [Online]. Available: <https://api.semanticscholar.org/CorpusID:264805175>
- [15] Q. Fan, H. Huang, M. Chen, H. Liu, and R. He, “Rmt: Retentive networks meet vision transformers,” *ArXiv*, vol. abs/2309.11523, 2023. [Online]. Available: <https://api.semanticscholar.org/CorpusID:262084150>
- [16] C. Li and C. Zhang, “Toward a deeper understanding: Retnet viewed through convolution,” 2023. [Online]. Available: <https://api.semanticscholar.org/CorpusID:261682326>
- [17] J. Ho, A. Jain, and P. Abbeel, “Denoising diffusion probabilistic models,” *ArXiv*, vol. abs/2006.11239, 2020. [Online]. Available: <https://api.semanticscholar.org/CorpusID:219955663>
- [18] C. Si, Z. Huang, Y. Jiang, and Z. Liu, “Freeu: Free lunch in diffusion u-net,” *ArXiv*, vol. abs/2309.11497, 2023. [Online]. Available: <https://api.semanticscholar.org/CorpusID:262064720>

- [19] R. J. Stegen, "Excitation coefficients and beamwidths of tschebyscheff arrays," *Proceedings of the IRE*, vol. 41, no. 11, pp. 1671–1674, 1953.
- [20] I. W. Selesnick and C. S. Burrus, "Generalized digital butterworth filter design," *IEEE Transactions on signal processing*, vol. 46, no. 6, pp. 1688–1694, 1998.

Appendix A: Gaussian Masks for Each Head in Different Blocks

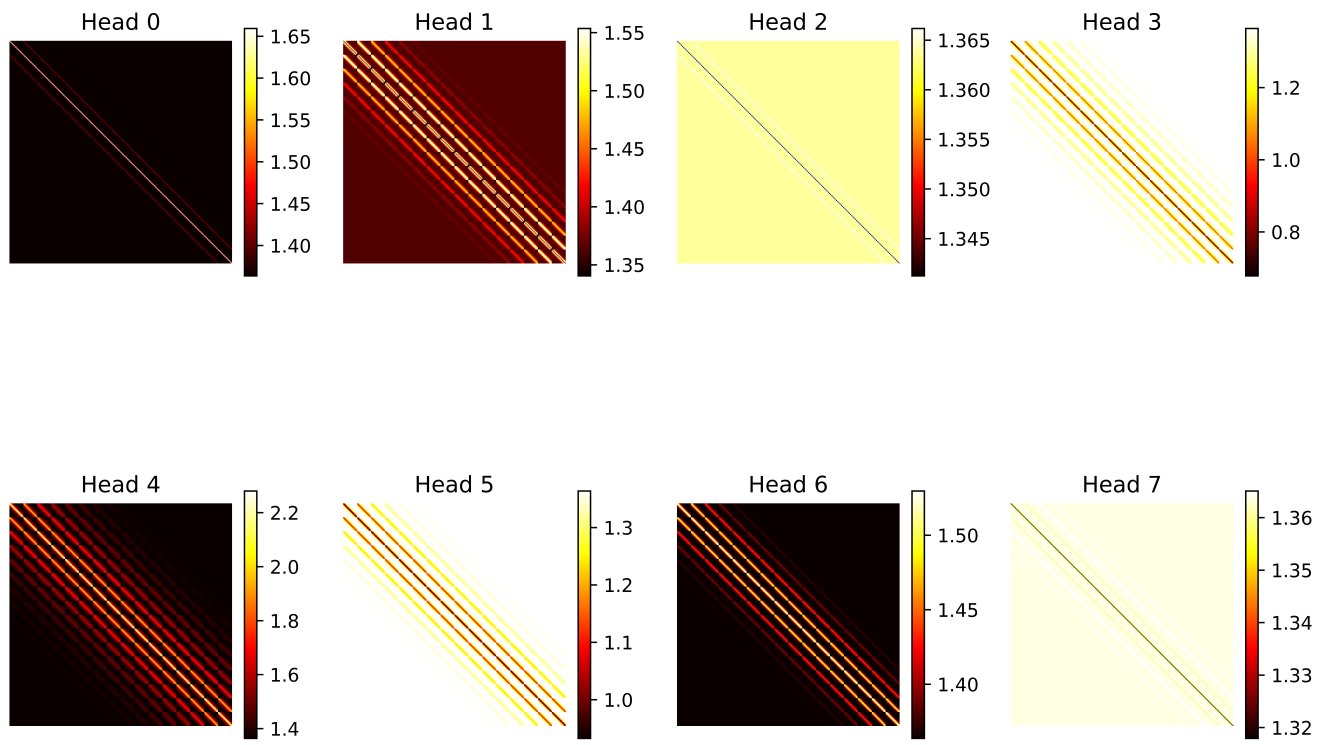


Figure 8: Gaussian Masks for Each Head in Decoder Block 1

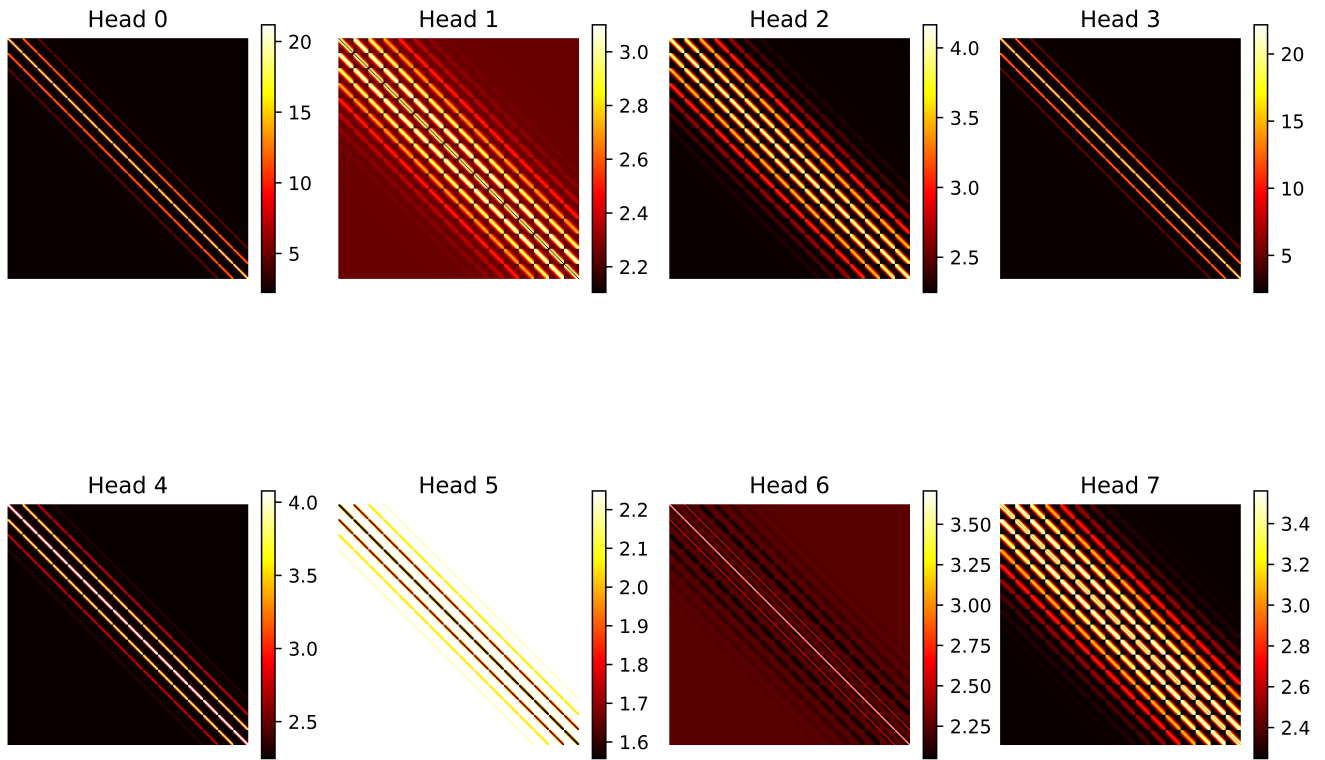


Figure 9: Gaussian Masks for Each Head in Decoder Block 2

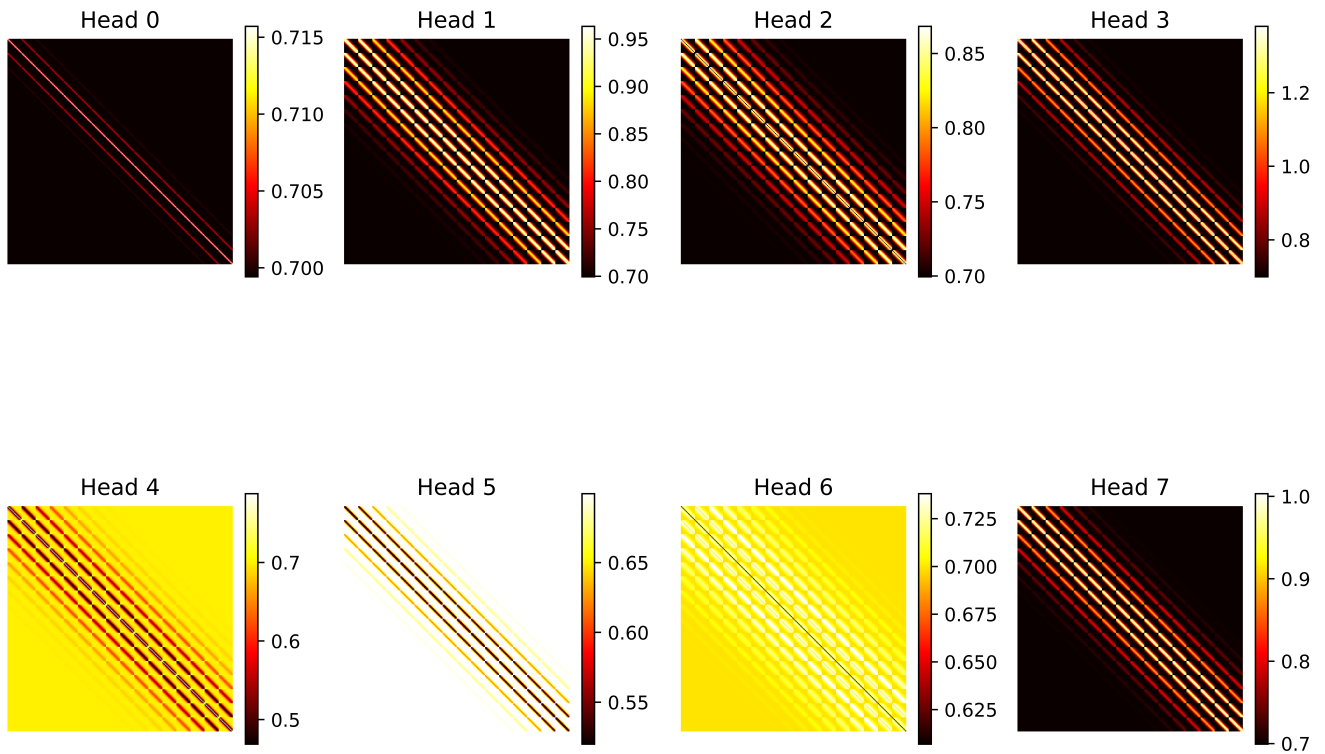


Figure 10: Gaussian Masks for Each Head in Decoder Block 3

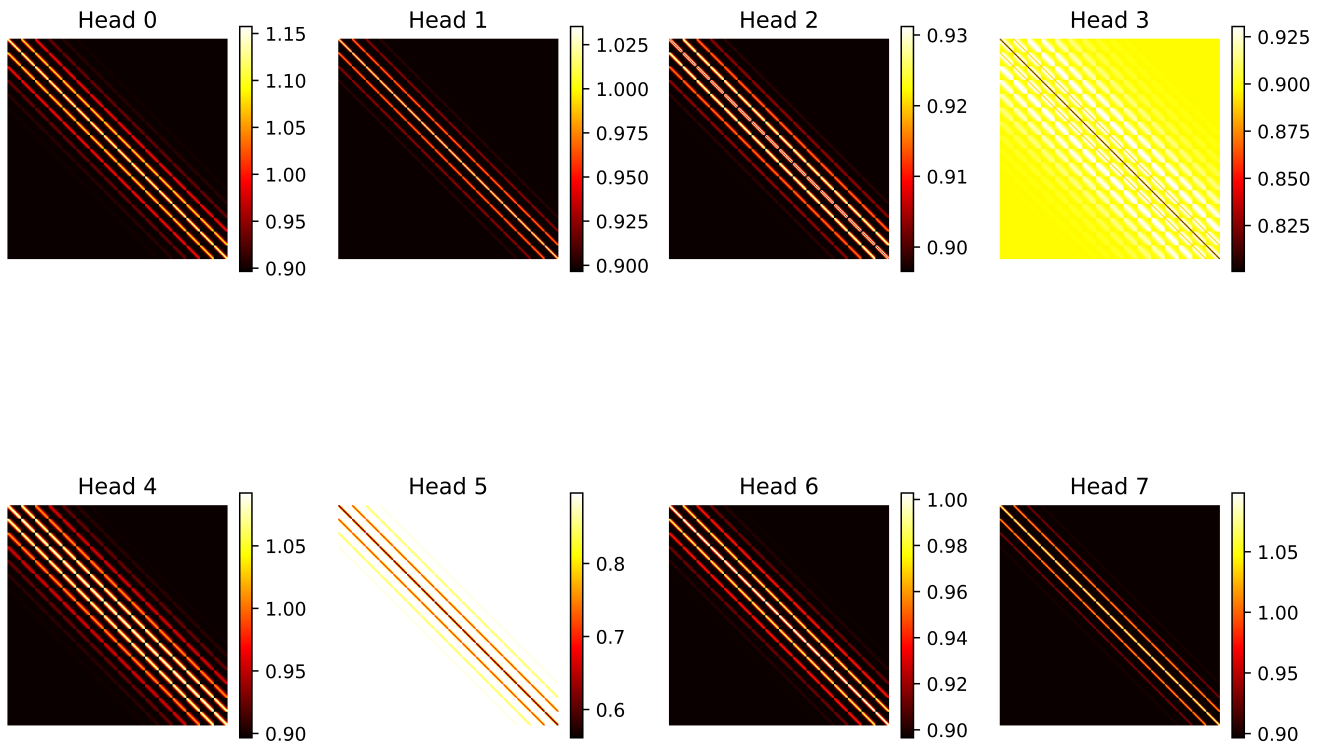


Figure 11: Gaussian Masks for Each Head in Decoder Block 4

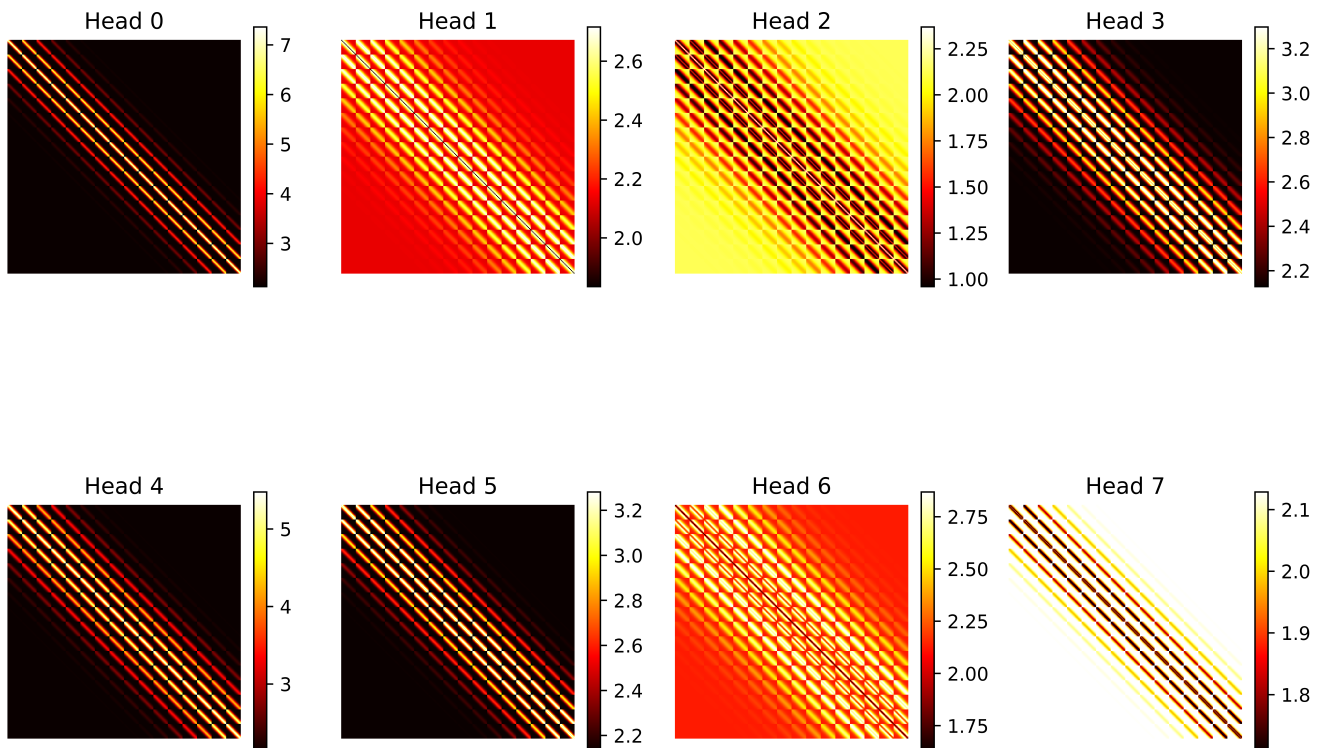


Figure 12: Gaussian Masks for Each Head in Decoder Block 5

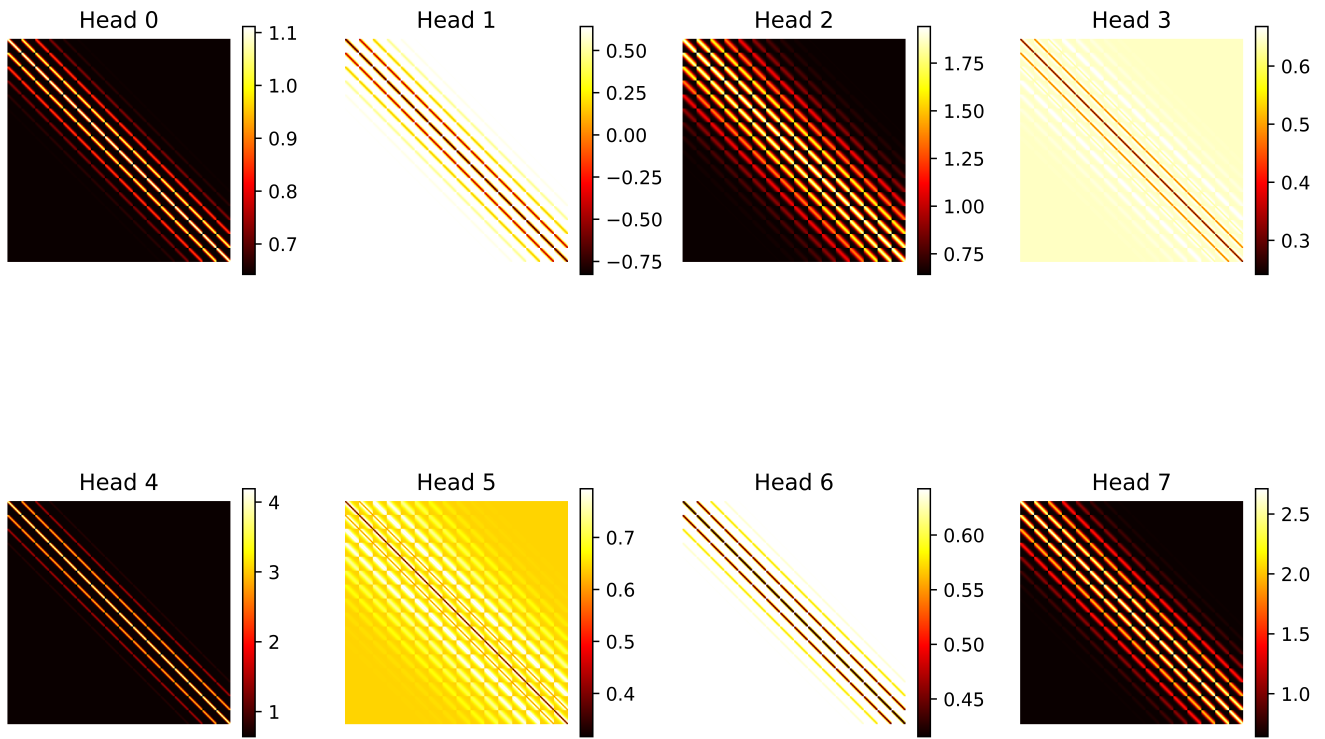


Figure 13: Gaussian Masks for Each Head in Decoder Block 6

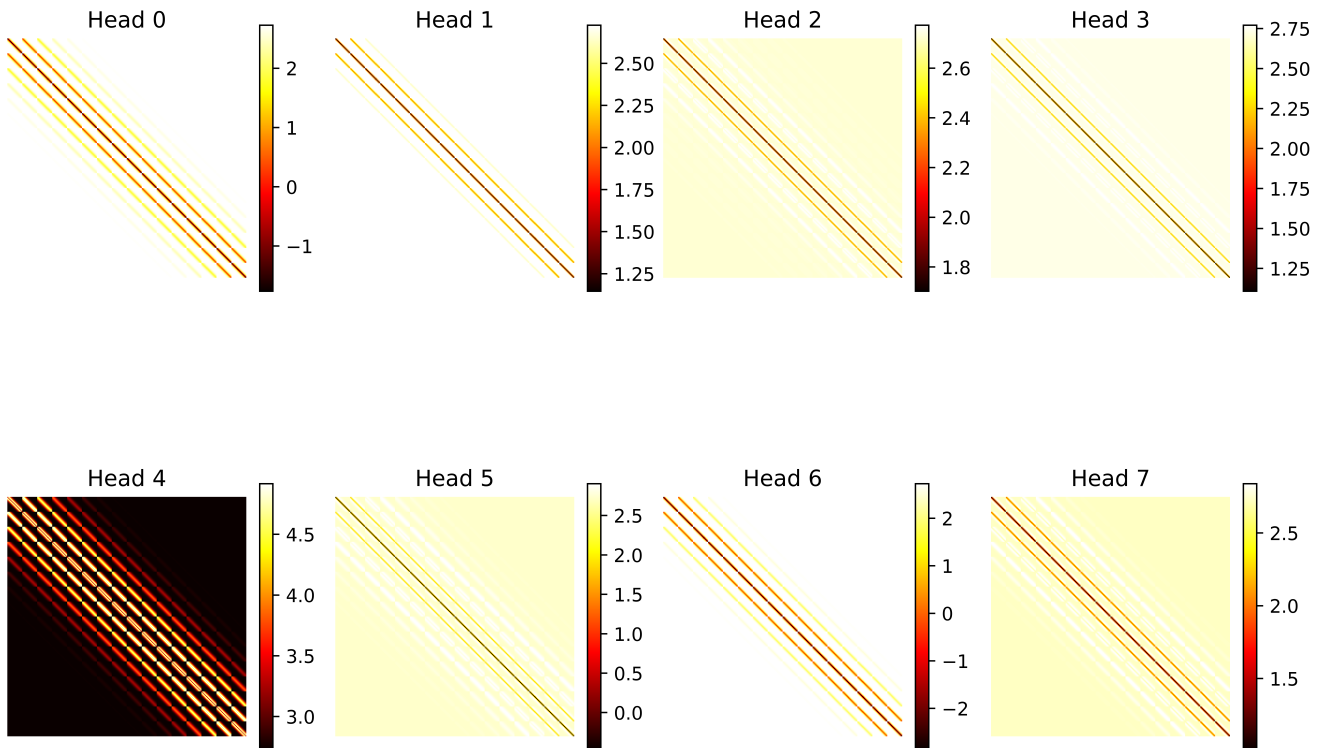


Figure 14: Gaussian Masks for Each Head in the Middle Block

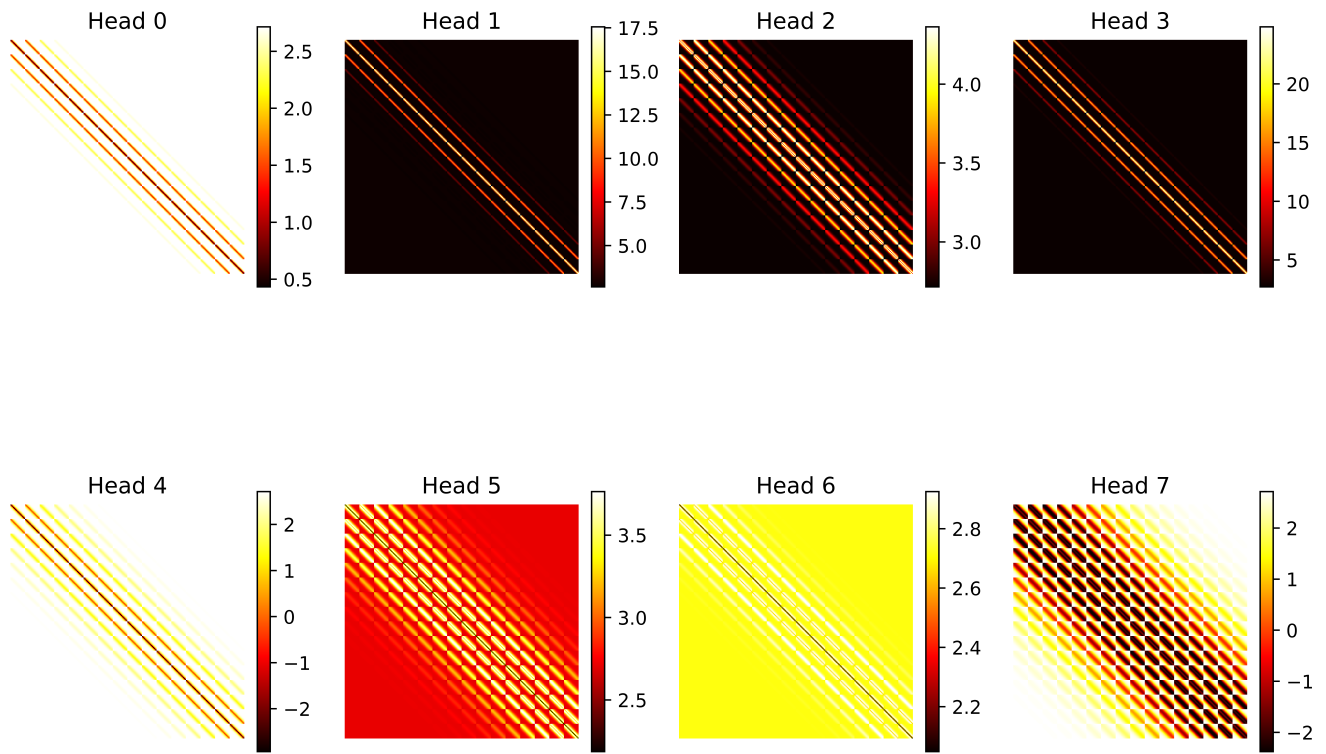


Figure 15: Gaussian Masks for Each Head in Encoder Block 1

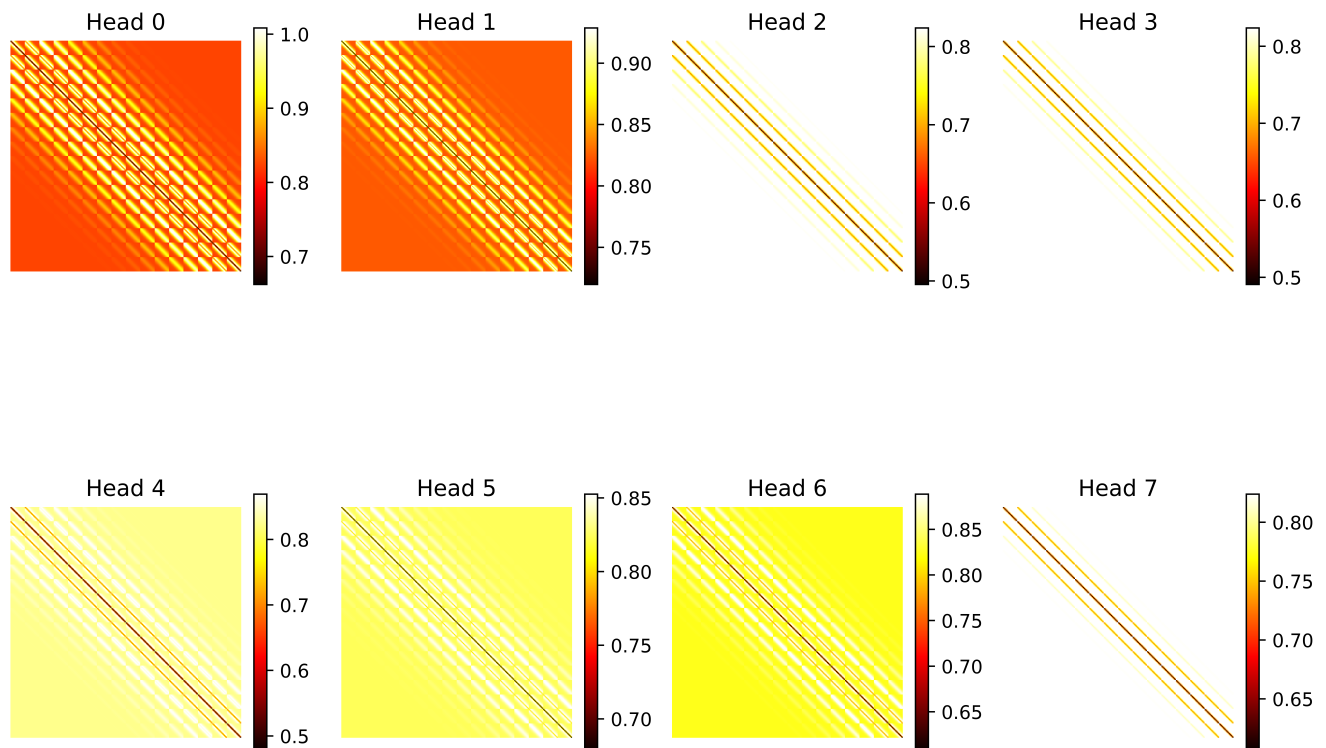


Figure 16: Gaussian Masks for Each Head in Encoder Block 2

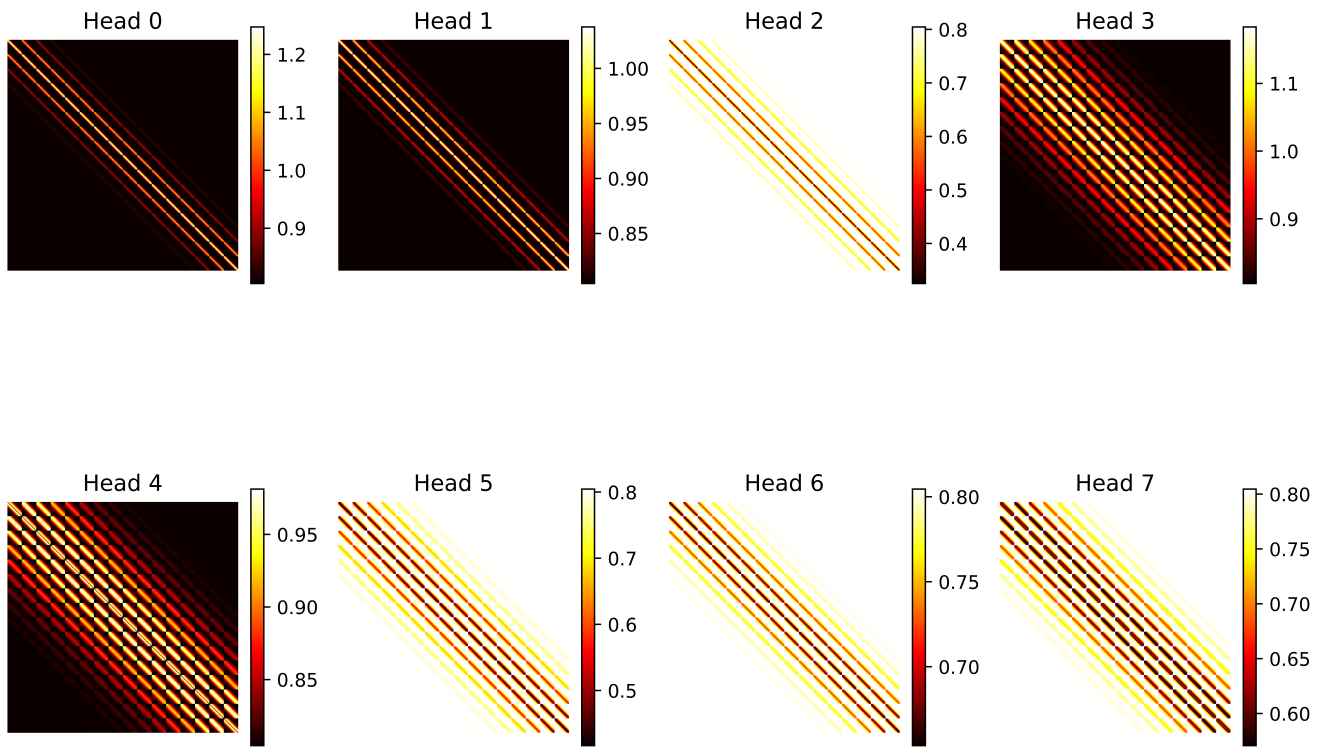


Figure 17: Gaussian Masks for Each Head in Encoder Block 3

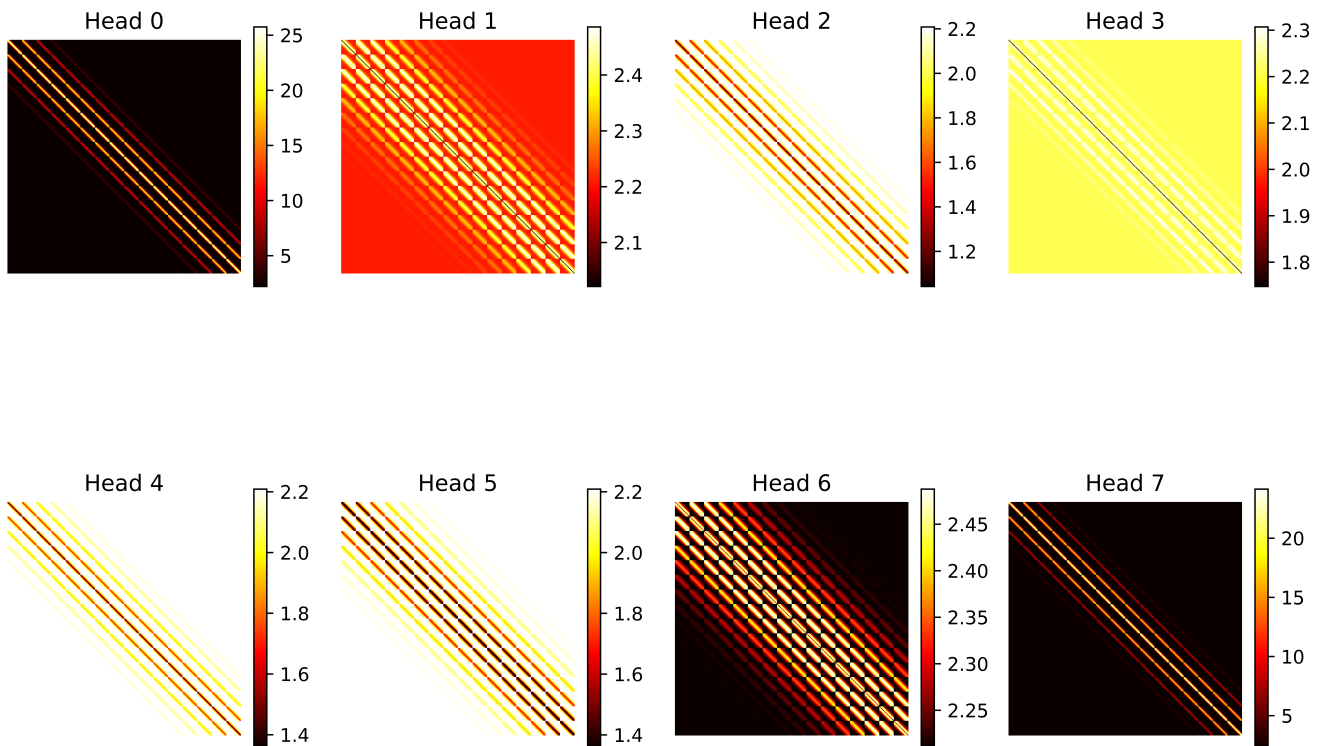


Figure 18: Gaussian Masks for Each Head in Encoder Block 4

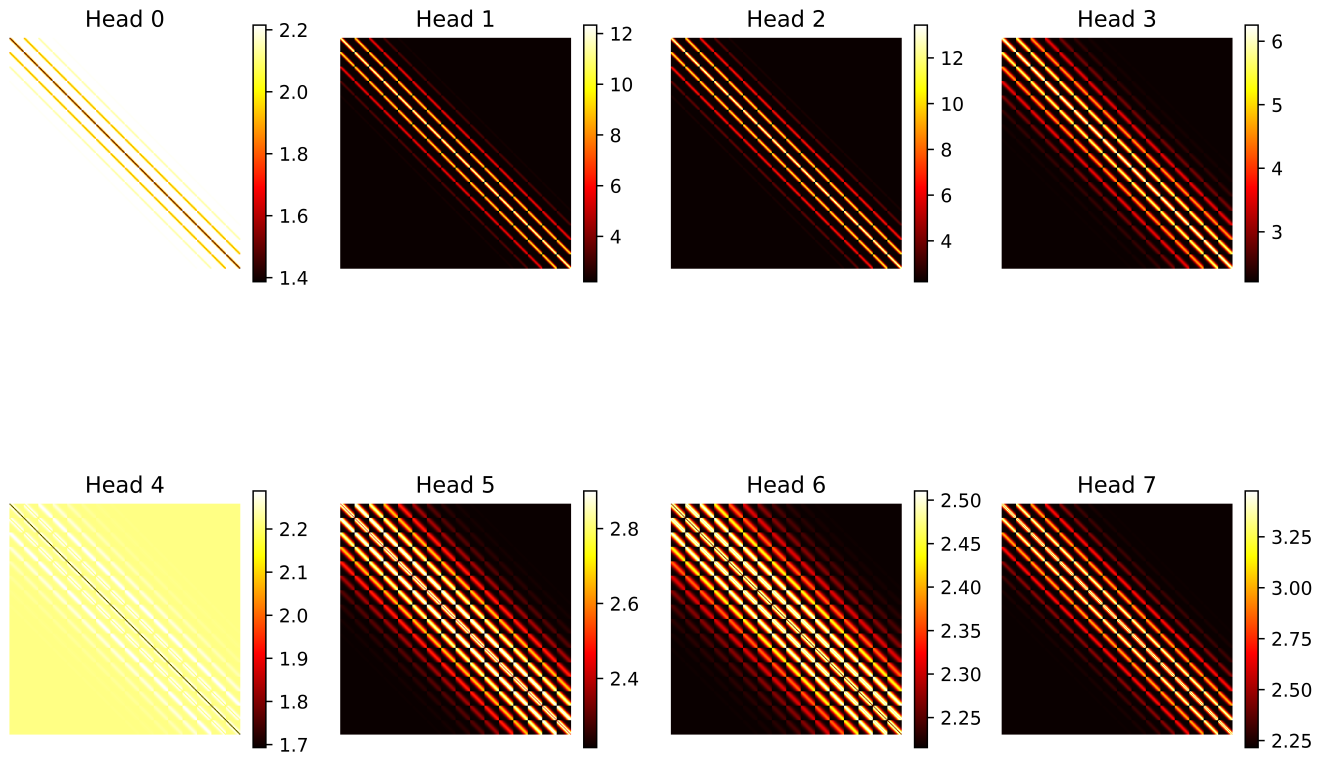


Figure 19: Gaussian Masks for Each Head in Encoder Block 5

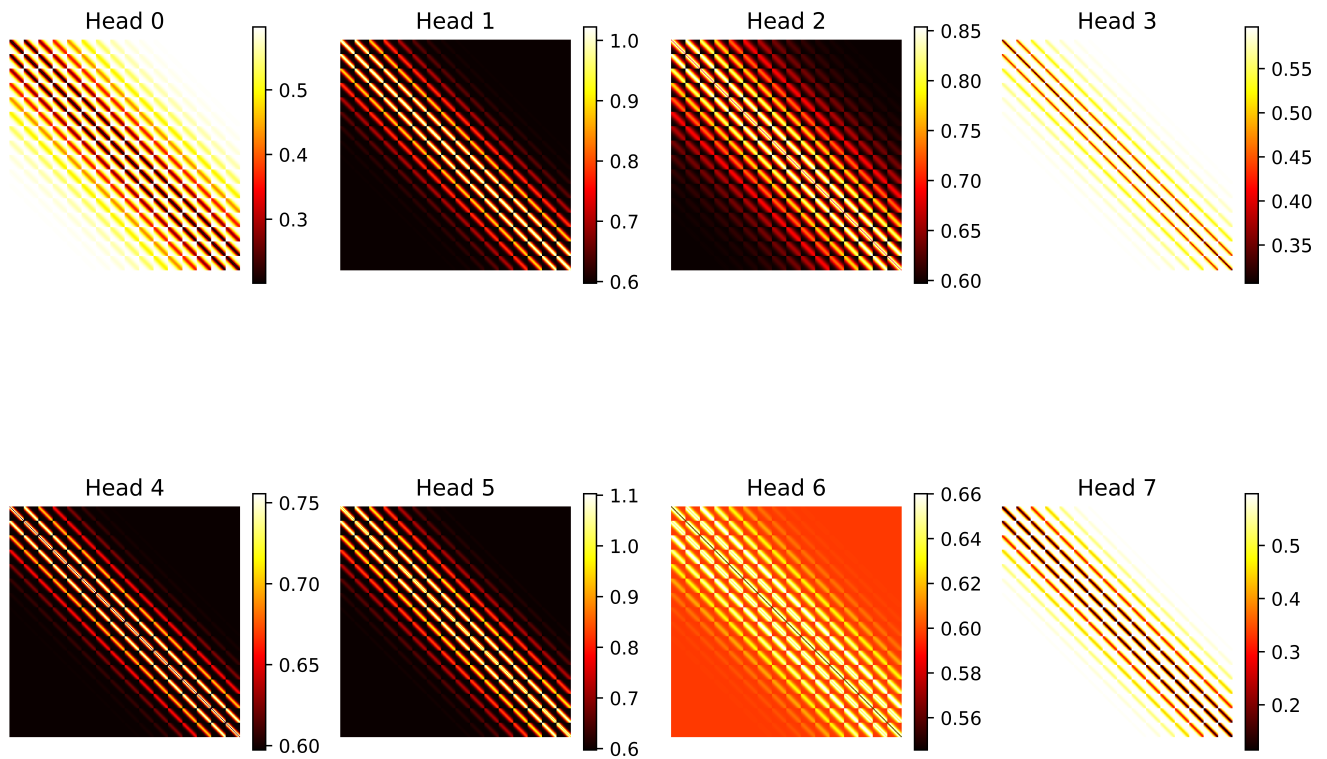


Figure 20: Gaussian Masks for Each Head in Encoder Block 6